RSC Advances

ROYAL SOCIETY OF CHEMISTRY

www.rsc.org/advances

RSC Advances

ARTICLE

The Efficient Adsorption Removal of Cr (VI) by Using Fe_3O_4 Nanoparticles Hybridized with Carbonaceous Materials

Received 01 June 2015,
Accepted 00th January 2015

DOI: 10.1039/x0xx00000x

www.rsc.org/

Hongtao Gao,*[a] Shuang Lv,[a] Jinbiao Dou,[a] Miaomiao Kong,[a] Dongmei Dai,[a] Chongdian Si[b] and Guangjun Liu[b]

Fe_3O_4 nanoparticles hybridized with carbonaceous materials, such as pinecone and graphene, were successfully synthesized by a facile hydrothermal method, which could be applied for Cr (VI) removal in aqueous solution. The nanocomposites were characterized by X-ray diffraction (XRD), scanning electron microscopy (SEM) and N_2 adsorption-desorption isotherm. Due to the combination of pinecone and graphene, both the surface properties and morphologies of Fe_3O_4 were modified. Fe_3O_4 spherical particles were distributed and firmly anchored on loose surface of pinecone or wrinkled graphene layers. The specific surface area increased from 23.85 to 27.86 and 121.17 $m^2 \cdot g^{-1}$ for Fe_3O_4/P and Fe_3O_4/G respectively. It enhanced the adsorption capacity for Cr (VI) of Fe_3O_4/P (62.5mg·g^{-1}) and Fe_3O_4/G (78.5mg·g^{-1}). The kinetics and isotherm study showed that the pseudo-second-order kinetic and Langmuir isotherm models could well fit the adsorption data. There were three steps in the adsorption process, such as the instantaneous adsorption step, the intraparticle diffusion and the final equilibrium stage. The reaction rate decreased along with temperature increasing, which indicated the adsorption for Cr (VI) was an exothermic process. The E_a were 34.39, 25.77 and 34.92 kJ·mol^{-1} for Fe_3O_4, Fe_3O_4/P and Fe_3O_4/G respectively, which illustrated the adsorption of Cr(VI) onto the surface of nanocomposite was a physical process. In no more than 5h, about 92.6% and 94% Cr(VI) were desorbed from the surface of Fe_3O_4/P and Fe_3O_4/G, respectively, which indicated the adsorption-desorption process for Cr(VI) was reversible, The results demonstrated that Fe_3O_4/P and Fe_3O_4/G exhibited excellent adsorption performance in the removal of Cr(VI). It was proved that carbonaceous materials, such as pinecone or graphene, could enhance the adsorption performance of Fe_3O_4, which might be used as adsorbent to remove heavy metal in industry effluent.

Introduction

Due to high chemical toxicity, bio-accumulative effect, without self-purification ability, easy migration and transformation, the heavy metal pollution has brought a serious threat to the ecological environment and human survival [1,2]. Among the various heavy metals, chromium (Cr) is one of the most toxic pollutants generated by the electroplating, metal processing and textile industries. Cr (VI) is more hazardous than Cr(III) as it can diffuse as CrO_4^{2-} or $HCrO_4^-$ through cell membranes and oxidize biological molecules[3]. At present, some physical and chemical methods, such as adsorption, ion exchange, dialysis, precipitation and extraction have been used to remove heavy metal ions from wastewater [4,5]. Among these methods, adsorption is one of the most economically favorable and effective technology.

Recently, a variety of adsorbents, have received much more attention for the removal of Cr (VI). Metal organic frameworks based on Cu-benzenetricarboxylates has been used for the adsorption of Cr(VI) from aqueous solution, whose maximum adsorption capacity was 48mg·g^{-1}.[6] The adsorption capacity of fly ash coated by chitosan for Cr(VI) was 36.22mg·g^{-1}.[7] A highly mesoporous melamine-formaldehyde resin showed enhanced adsorption capacity (66.65 mg·g^{-1}) and selectivity for Cr(VI) [8]. $BaTiO_3$@SBA-15 nanocomposite was used as an adsorbent for the removal of Cr(VI)-contaminated water and it showed an adsorption capacity of 98.2 wt% within only 40 min contact time in a batch reactor. [9]

Fe_3O_4 nanoparticles with various controlled morphologies own some unique physicochemical properties, such as variable electronic structures, large specific surface area, and good adsorption ability. Moreover, due to its easy synthesis and magnetic property which makes it be easily separable, Fe_3O_4 magnetic nanoparticles have attracted much interest. Fe_3O_4 nanocrystals showed excellent electrochemical sensing performances toward heavy metal ions. [10,11] Magnetic gelatin showed an excellent adsorption capacity to offer rapid Cr(VI) removal from water within 50 min[12].The adsorption efficiency of Fe_3O_4 magnetic particles for Cr(VI) was enhanced in the absence of ultrasound. Some strategies, such as combination with other metal oxide, structure and surface modification, have been adopted to improve adsorption efficiency and

Laboratory of Inorganic Synthesis and Applied Chemistry, College of Chemistry and Molecular Engineering, Qingdao University of Science & Technology, Qingdao, 266042, P. R. China, E-mail: gaohtao@126.com; Tel: +86- 0532-84022681
Department of Chemistry and Chemical Engineering, Jining University, Qufu 273155, China.

capacity of Fe_3O_4 for heavy metal contaminant. 3-aminopropyltriethoxysilane was used to regulate the surface of magnetic Fe_3O_4 to enhance the adsorption efficiency of metal ions[13]. Easily separable humic acid coated magnetite nanoparticles were employed for effective adsorption and reduction of toxic Cr(VI) to nontoxic Cr(III) [14].

The properties of Fe_3O_4 could be modified by combining with carbon materials. Magnetic iron oxide chitosan composites have been widely used for the treatment of water polluted with metal and organic materials[15]. Pine bark waste was used to prepare magnetic biochar composite for adsorption removal of Pb(II) and Cd(II)[16].The maximum adsorption capacity of magnetic chitosan nanoparticles was calculated as 55.80mg·g^{-1}, for removal of Cr(VI) from aqueous solution[3]. G. Yang reported a novel nitrogen-functionalized magnetic ordered mesoporous carbon, which was proved to be a superior adsorbent for simultaneous removal of lead and phenol contamination from water[17]. Iron oxide nanoparticles-doped carboxylic ordered mesoporous carbon was proved to be excellent treatment agent for rapid adsorption of organic pollutants from industrial effluents[18]. Polyacrylonitrile-based activated carbon fibers [19], and imidazolium ionic liquid functionalized magnetic carbon nanotubes exhibited high adsorption sensitivity, selectivity and capacity in removal Cr(VI) from water[20].

Owing to excellent conductivity, superior chemical stability and high specific surface area, graphene has attracted a great deal of attention in recent years. By hybridizing with graphene sheets, the adsorption performance porous Fe_3O_4 hollow microspheres were enhanced, and the maximum sorption capacity for Cr(VI) was 32.33 mg·g^{-1}. [21,22] The surface charge-tunable Fe_3O_4 nanoparticles for removal of dye pollutants was enhanced by reversibly binding to graphene[23]. The water-soluble Fe_3O_4 nanoparticles could disperse onto graphene uniformly [24]. The interaction between the graphene and Fe_3O_4 particles could prevent graphene nanosheets from restacking and Fe_3O_4 particles from agglomeration.

In this paper, environment-friendly carbon materials, such as pinecone and graphene, have been hybridized with Fe_3O_4 nanoparticles to improve the adsorption efficiency and capacity for Cr (VI). The products were characterized by X-ray diffraction (XRD), scanning electron microscopy (SEM) and nitrogen adsorption-desorption isotherm. Batch experiments was carried out to investigate the adsorption performance of nanocomposites for the removal of Cr(VI) from aqueous solution. Furthermore, the adsorption kinetics and isotherms, intraparticle diffusion process, thermodynamics and the mechanism of sorption reaction have also been investigated. Not only Fe_3O_4/pinecone (Fe_3O_4/P) but also Fe_3O_4/graphene (Fe_3O_4/G) exhibited more excellent adsorption performance in the removal of Cr(VI), compared to pristine Fe_3O_4. It indicated that hybridization of carbonaceous materials could improve the adsorption performance for heavy metal ions.

Experimental

Materials

All the chemicals were of analytical grade and used without further purification. The pinecone was calcined in the muffle furnace at the temperature of 400□ for 3h. Then the obtained powder was used as biochar carbonaceous material to prepare the adsorbent. The graphene used in this work was synthesized by modified Hummer method[25].

Synthesis of absorbents

A typical synthesis process for the Fe_3O_4/P and Fe_3O_4/G nanocomposites were as follows: 0.0645g pinecone powder (or 0.002g graphene after sonicated), the 1.35g ferric chloride hexahydrate ($FeCl_3·6H_2O$) and 3.60g sodium acetate (CH_3COONa) were added into a solution mixed from 49 mL ethylene glycol and 0.6 mL H_2O. The solution was transferred into a teflon-lined high-pressure reaction autoclave after stirred for 30 min. And after having been maintained at given temperature for several hours, the autoclave was naturally cooled to the ambient temperature. The obtained sample was separated from the autoclave, washed by distilled water and ethanol several times successively, and then dried in an oven at 100°C for 12 hours to obtain the magnetic nanocomposites.

Characterization

X-ray diffraction (XRD) was carried out to identify the crystal phase composition of synthesized samples over the 2θ range from 10° to 70° using a Bruker D8 advance X-ray diffractometer with Cu Kα radiation (λ=1.54056 Å) operated at 45 kV and 40 mA. The surface morphology of the product was characterized with a scanning electron microscope JSM-6300 (JEOL Ltd, Japan). In addition, the N_2-based Brunauer Emmett Teller (BET) surface area of products was determined by the surface area analyzer (ASAP 2020 V4.01). UV–vis spectrophotometer (Cary 50, Varian Co. USA) was used to monitor the removal of Cr(VI) in the reaction process.

Adsorption experimental

The adsorption performance of the as-prepared samples was evaluated by adsorption removal of Cr (VI) in aqueous solution. In a typical adsorption experimental process, Fe_3O_4 nanocomposite adsorbent (0.20 g) was added to the aqueous solution containing Cr (VI) (100mL, 50 mg·L^{-1}). The suspension was placed in the constant-temperature shaker (150 r/min) at the water bath of 25 °C. At the given time intervals, 1.0 mL of aqueous suspension was taken out, centrifuged and filtered through a 0.45 μm millipore filter to determine the concentration of Cr(VI). And the concentration of Cr(VI) in the adsorption process was measured using a UV–vis spectrophotometer (Cary 50) at a wavelength of 540nm by diphenylcarbazine method.[26]

The removal efficiency of Cr(VI) was calculated by Eq.(1):

$$Cr(\mathrm{VI})\% = \frac{C_0 - C_t}{C_0} \times 100\% \qquad (1)$$

The amount of adsorbed Cr(VI) at time *t* was calculated according to the Eq. (2):

$$q_t = \frac{(C_0 - C_t)V}{m} \qquad (2)$$

where C_0 and C_t (mg·L^{-1}) are the concentration of Cr(VI) initially and at any time *t*, q_t (mg·g^{-1}) is the adsorption capacity at any time *t*, *V* (L) is the volume of the Cr(VI) solution and *m*(g) is the quality of the adsorbent used.

Adsorption kinetics

The adsorption kinetics are of great importance for adsorption investigation because they can indicate the adsorption rate of the

heavy metal ions removal from aqueous solutions and supply effective data for comprehending the mechanism of adsorption reactions[27,28]. The linear forms of the pseudo-first-order kinetic model and the pseudo-second-order kinetic model were applied to investigate adsorption mechanism. The linear form of the first-order kinetic rate model was expressed as Eq. (3)[29]:

$$\log(q_e - q_t) = \log q_e - \frac{k_1}{2.303}t \qquad (3)$$

And the linear form of the pseudo-second-order kinetic rate model was expressed as Eq. (4)[30]:

$$\frac{t}{q_t} = \frac{1}{k_2 q_e^2} + \frac{t}{q_e} \qquad (4)$$

Where k_1 (min^{-1}) is the rate constant for first-order adsorption, k_2 ($g \cdot mg^{-1} \cdot min^{-1}$) is the rate constant for second-order adsorption, q_e ($mg \cdot g^{-1}$) is the adsorption capacity at equilibrium, and q_t ($mg \cdot g^{-1}$) is the adsorption capacity at any time t. The adsorption capacity of Cr(VI) on the adsorbent can be calculated by the adsorption isotherms.

Results and discussion

XRD analysis

The crystal structure of product was examined by XRD. The XRD patterns for Fe_3O_4, Fe_3O_4/P and Fe_3O_4/G samples were presented in Fig. 1. The peaks, which lied at 31.2°, 36.8°, 38.1°, 44.7°, 55.6°, 59.3° and 65.2°, corresponding to (220), (311), (222), (400), (422), (511) and (440) planes of the standard card of cubic Fe_3O_4 (JCPDS#26-1136). Compared to the XRD pattern of Fe_3O_4, the peaks lied at 31.2°, 36.8°, and 65.2° almost disappeared completely, the highest peak lied at 38.1° weakened and broadened. There appeared new peaks at 34.0°, 57.9° and 63.5° in the XRD pattern of Fe_3O_4/P. All of these diversities can be attributed to the hybridization of pinecone, which caused crystal structure and crystallinity varied. There appeared a peak lied at 20.8° in the XRD pattern of Fe_3O_4/G, which could prove that graphene was hybridized into the product [31]. Compared to the XRD pattern of Fe_3O_4, the peaks lied at 31.2°, 36.8°, 38.1°, 44.7°, 55.6°, 59.3° and 65.2° all became sharp, which indicated that the product crystallized well. The hybridization of graphene was favorable to the crystal growth of product.

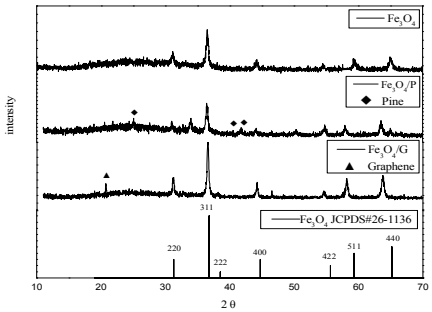

Fig. 1. XRD patterns for the Fe_3O_4, Fe_3O_4/P and Fe_3O_4/G.

SEM analysis

The SEM image of the Fe_3O_4 was presented in Fig. 2a, from which could be seen that the spherical Fe_3O_4 dispersed uniformly with size ranging from 100 to 200nm. Fig.2b was the enlarged image of Fe_3O_4, it could be seen that the rough surface provided more active adsorption sites, which might own the high adsorption performance. Fig. 2c presented the SEM image of pinecone powder calcined at 400℃. It could be seen that the surface morphology of the carbonaceous material was loose and porous, which might support Fe_3O_4 on its surface. The SEM image of Fe_3O_4/P was showed in Fig. 2d, from which could be seen that Fe_3O_4 was loaded tightly on the surface of the calcined pinecone, which acted as supporting matrix. Fig. 2e presented the SEM image of graphene, which was smooth flake with much wrinkles. Fig. 2f presented SEM image of Fe_3O_4/G, which indicated that Fe_3O_4 spherical particles were distributed and firmly anchored onto the wrinkled graphene layers. This structure increased the contact surface of Fe_3O_4 to react with heavy metal. It would enhance the adsorption efficiency of Fe_3O_4/G for heavy metal ions.

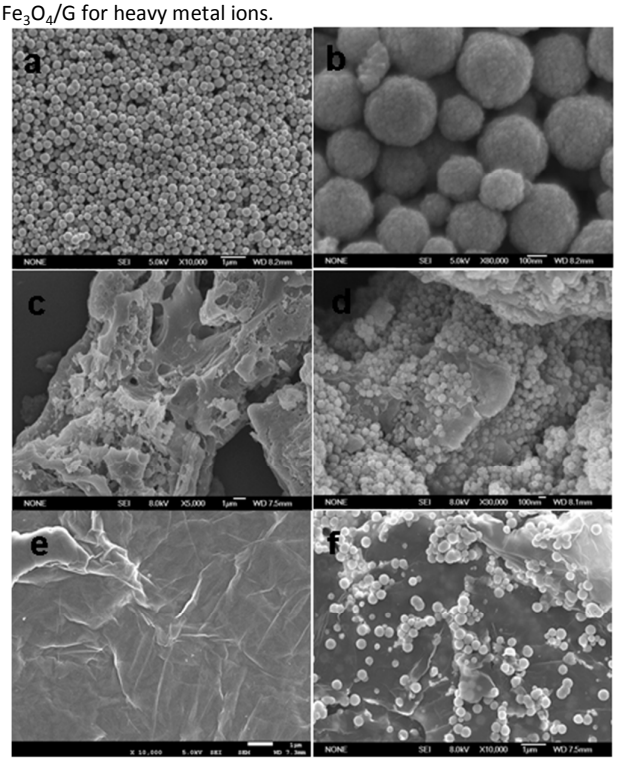

Fig. 2. SEM images of (a) Fe_3O_4 (b) Fe_3O_4 (enlarged scale), (c) Pinecone powder, (d Fe_3O_4/P, (e) Graphene, (f) Fe_3O_4/G.

Specific surface area

Fig. 3 showed the N_2 adsorption-desorption isotherm curves for the samples. The specific surface area of Fe_3O_4, Fe_3O_4/P and Fe_3O_4/G was respectively 23.85, 27.86 and 121.47 $m^2 \cdot g^{-1}$. And the pore sizes were 9.26, 21.02 and 14.64 nm for Fe_3O_4, Fe_3O_4/P and Fe_3O_4/G respectively. The combination of calcined porous pinecone increased the pore size of Fe_3O_4, and the hybridization of graphene increased greatly the BET surface area of Fe_3O_4, which could improve the adsorption efficiency of Fe_3O_4. It indicated that Fe_3O_4 nanoparticles hybridized with carbonaceous materials, such as calcined porous pinecone and graphene, might improve adsorptive performance of Fe_3O_4 for heavy metal ions.

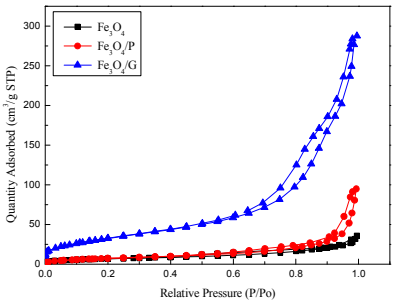

Fig. 3. Nitrogen adsorption-desorption isotherms of Fe_3O_4, Fe_3O_4/P, Fe_3O_4/G.

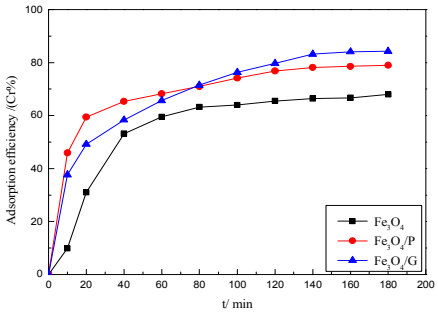

Fig. 4. Adsorption efficiency of Cr(VI) on Fe_3O_4, Fe_3O_4/P and Fe_3O_4/G.

Adsorption efficiency

Fig. 4 presented the adsorption removal efficiency of Cr(VI) (50mg·L^{-1}) in aqueous solution at 25□. The adsorption rates of nanomaterials for Cr (VI) were rapid at the first 20min, and then the adsorption curve became flat, eventually reached the adsorption equilibrium in about 3h. The removal efficiency for Cr(VI) of Fe_3O_4, Fe_3O_4/P and Fe_3O_4/G were 67.8%, 79.5% and 84.6%, respectively. It indicated that the hybridization of pinecone or graphene enhanced the adsorption efficiency of Fe_3O_4 significantly.

For the desorption process, the Cr(VI) loaded nanocomposite was dispersed into 100 mL NaOH (0.10 mol·L^{-1}) aqueous solution and shaken at 150rpm for 5h. When desorption equilibrium was reached, about 90%, 92.6% and 94% Cr(VI) were desorbed from the surface of Fe_3O_4, Fe_3O_4/P and Fe_3O_4/G, respectively. It indicated that the adsorption-desorption process was nearly reversible, which illustrated the adsorption of Cr(VI) on the adsorbent surface was a physical process.

Adsorpton kinetics

The pseudo-first-order kinetic line plots of *log(q_e-q_t) versus t* are shown in Fig. 5a and the pseudo-second-order kinetic line plots of *t/q_t versus t* were shown in Fig. 5b. The kinetic constants were listed in Table 1. $q_{e,cal}$ and $q_{e,exp}$ were calculated and experimental adsorption capacities at equilibrium respectively. The R^2 of the first-order kinetic model were all less than 0.926 and those of the second-order kinetic model were all more than 0.996. It indicated that the second-order adsorption kinetic model fit the adsorption process better than the first-order kinetics model. And significantly, there was a good agreement between the calculated and experimental q_e values, confirming the applicability of the second-order adsorption kinetic model to describe the adsorption process.

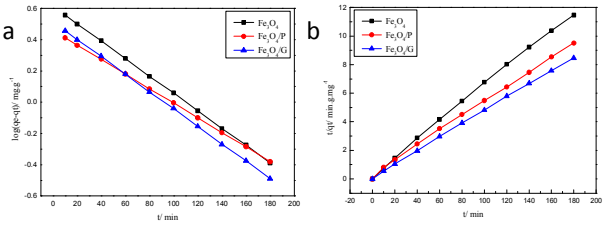

Fig. 5. Pseudo- first-order kinetics (a) and second-order kinetics (b) for adsorption of Cr(VI) onto Fe_3O_4, Fe_3O_4/P and Fe_3O_4/G.

Table 1. kinetic constants of Cr(VI) adsorption onto Fe_3O_4, Fe_3O_4/P and Fe_3O_4/G

Samples	$q_{e,exp}$ /(mg·g^{-1})	Pseudo-first-order			Pseudo-second-order		
		$q_{e,cal}$ /(mg·g^{-1})	k_1 / (min^{-1})	R^2	$q_{e,cal}$ /(mg·g^{-1})	k_2 / (min^{-1})	R^2
Fe_3O_4	15.66	17.56	0.0128	0.879	15.63	0.0192	0.998
Fe_3O_4/P	19.29	20.84	0.0106	0.926	19.33	0.0211	0.998
Fe_3O_4/G	20.37	17.80	0.0096	0.873	20.29	0.0236	0.996

Table 2. Intraparticle diffusion kinetics constants

Sample	k_1/ (g·mg^{-1}·min^{-1})	k_2 /(g·mg^{-1}·min^{-1})	k_3 / (g·mg^{-1}·min^{-1})	R_1^2	R_2^2	R_3^2
Fe_3O_4	5.25	0.248	0.0588	0.978	0.969	0.994
Fe_3O_4/P	6.01	0.529	0.0728	0.998	0.996	0.990
Fe_3O_4/G	6.88	0.673	0.136	0.995	0.987	0.985

Intraparticle diffusion analysis

The intraparticle diffusion kinetic model based on the Weber-Morris equation [Eq. (5)] was further used to investigate the control step of the process and to clarify the mechanism of adsorption[32]:

$$q_t = K_{di} t^{1/2} + C_i \qquad (5)$$

Where K_{di} (g·mg^{-1}·$min^{1/2}$) is the rate parameter during stage *i*, which is calculated from the slope of the straight line of q_t versus $t^{1/2}$, C_i is the intercept during stage *i*, which gives an idea about the thickness of the boundary layer. For the intraparticle diffusion, q_t *versus* $t^{1/2}$ will be linear. The linear fits of intraparticle diffusion model for the adsorption of Cr(VI) onto products were presented in Fig. 6. The plots exhibited three-linearity, implying there were three steps in

the adsorption process. The slope of three stages (K_{d1}> K_{d2}> K_{d3}) were listed in Table 2 and the values of K determined the adsorption speed. The first stage, which was completed within 10 minutes, was related to the instantaneous adsorption step that mainly occurred on the external surface of the adsorbents. This arose from the fact that the initial Cr(VI) concentration in the solutions was high and this large concentration gradient provided enough driving force for Cr(VI) diffusing to the external surface of the adsorbents. It was evident that K_{d1} values for Fe_3O_4/P and Fe_3O_4/G was greater than that of Fe_3O_4, which could be seen from table 2. It was understandable by taking account of larger specific surface areas for Fe_3O_4/P and Fe_3O_4/G contrast to Fe_3O_4. The second adsorption stage was a relatively slow region, which was related to the intraparticle diffusion. It was a rate-limiting step. The third region was the final equilibrium stage. Since the final concentrations of Cr(VI) left in the solutions was extremely low, the intraparticle diffusion further slowed down. As discussed above, Cr(VI) was slowly transported by intraparticle diffusion into the particles and finally reached the surface of nanomaterials. Table 2 presented a comparison of intraparticle diffusion rate parameters for the adsorption of Cr(VI) on Fe_3O_4, Fe_3O_4/P and Fe_3O_4/G. The K_{d1} values of Fe_3O_4/P and Fe_3O_4/G were larger than that of Fe_3O_4 owing to the former having larger surface areas. Further observation indicated K_{d1}> K_{d2}> K_{d3}, which was not surprising because the concentration of Cr(VI) left in the solutions gradually decreased with prolonging adsorption time.

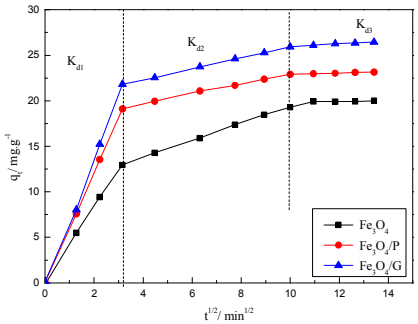

Fig.6. The intraparticle diffusion kinetics of Cr(VI) on Fe_3O_4, Fe_3O_4/P and Fe_3O_4/G.

Adsorption isotherms

To fully understand the adsorption process, several different isotherm models, such as the Langmuir, Freundlich and Temkin isotherm models, are considered. Fitting experimental data to appropriate isotherm model is a very important step, because the results give information about the interactions of adsorbate with the adsorbent.

The Langmuir isotherm

The Langmuir equation is expressed as Eq. (6):

$$\frac{C_e}{q_e}=\frac{C_e}{q_{\max}}+\frac{1}{K_L q_{\max}} \qquad (6)$$

where C_e (mg·L^{-1}) is the equilibrium concentration of Cr(VI) in solution, q_e (mg·L^{-1}) is the equilibrium capacity of Cr(VI) on the adsorbent, q_{max} (mg·g^{-1}) is the theoretical maximum monolayer sorption capacity, and K_L (L·mg^{-1}) is the Langmuir constant, which is related to the free energy of adsorption. The constants of q_{max} and K_L could be obtained from the intercept and the slope of the linear plot of C_e/q_e *versus* C_e (Fig. 7).

The Freundlich isotherm

The linear form of the Freundlich equation is written as Eq. (7):

$$\ln q_e=\ln K_F+\frac{1}{n}\ln C_e \qquad (7)$$

where K_F[(mg·g^{-1})(L·mg^{-1})$^{1/n}$] is the Freundlich constant related to the bonding energy. *1/n* is a heterogeneous adsorption factor. The constants K_L and n can be obtained from the intercept and the slope of the linear plots of lnqe versus lnC_e (Fig. 8). The Freundlich exponent n of Fe_3O_4, Fe_3O_4/P and Fe_3O4/G respectively were 1.89, 2.45 and 2.70 by calculation, where n>1 implied a favorable adsorption condition. The results indicated that the adsorption process of Fe_3O_4, Fe_3O_4/P and Fe_3O_4/G were reversible.

The Temkin isotherm

The Temkin adsorption isotherm is described as follows (Eq.8):

$$q_e=B\ln K_t+B\ln C_e \qquad (8)$$

Where K_t (L·g^{-1}) is the equilibrium constant related to the maximum binding energy and B is related to the heat of adsorption. The linear plots of q_e *versus* lnC_e were shown in Fig. 9.

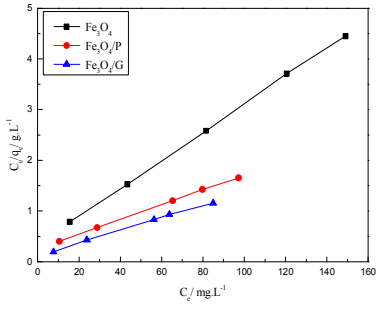

Fig.7. Langmuir linear plots for adsorption of Cr(VI) on Fe_3O_4, Fe_3O_4/P and Fe_3O_4/G).

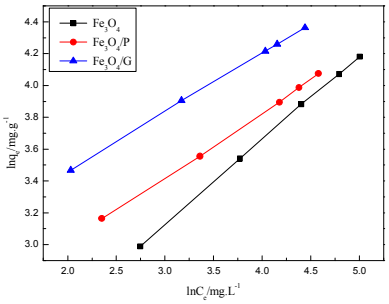

Fig.8. Freundlich linear plots for adsorption of Cr(VI) on Fe_3O_4, Fe_3O_4/P and Fe_3O_4/G.

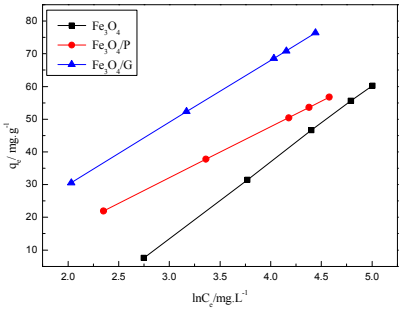

Fig.9. Temkin linear plots for adsorption of Cr(VI) on Fe_3O_4, Fe_3O_4/P and Fe_3O_4/G.

Overall, the relative parameters calculated from the three models were listed in Table 3. The higher correlation coefficient of the Langmuir model illustrated that the adsorption data were better fitted by the Langmuir model (R^2 >0.992) than by the Freundlich model and the Temkin model. Then, it showed that the adsorption occurred in a monolayer and at a fixed number of identical adsorption sites. It meant that there was no formation of chemical bonds between chromium and adsorbent. Furthermore, the Freundlich constant n values were greater than 1, which confirmed that the adsorption process could be considered as Langmuir adsorption. Hence, we could obtain the calculated q_{max} of Fe_3O_4, Fe_3O_4/P and Fe_3O_4/G were 39.5, 62.5 and 78.5 mg·g^{-1}, respectively.

Adsorption thermodynamics

The thermodynamics supposes that in an isolated system, where energy could not be gained or lost, the entropy change is the driving force. The Arrhenius equation has been applied to measure the activation energy of adsorption, which represents the minimum energy that reactants must have for the reaction to proceed, as expressed in Eq.9[33]:

$$\ln k_2 = \ln A - \frac{E_a}{RT} \qquad (9)$$

where E_a (kJ·mol^{-1}) is the Arrhenius activation energy, A is the Arrhenius factor, R (8.314 J·mol^{-1}·K) is the gas constant and T(K) is the absolute temperature. When lnk_2 was plotted against $1/T$, a straight line with the slope $-E_a/R$ was obtained (Fig. 10). Table 4 presented Kinetic constants of activation energy in adsorption. The q_e decreased along with increasing temperature, which indicated the adsorption for Cr(VI) was an exothermic process. The magnitude of activation energy gives an idea about the type of adsorption such as chemical or physical adsorption. The physical processes often have activation energies in the range of 0–40 kJ.mol^{-1}, yet higher activation energies (40–800 kJ·mol^{-1}) imply chemisorption[34]. The E_a values were 34.39, 25.77 and 34.92kJ·mol^{-1} for Fe_3O_4, Fe_3O_4/P and Fe_3O_4/G respectively, which indicated that the adsorption of Cr(VI) on all samples were physical adsorption.

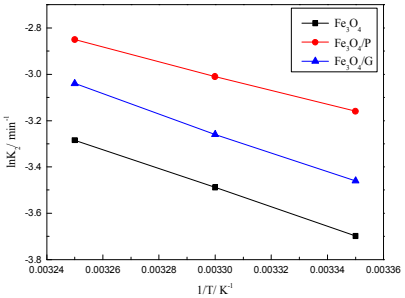

Fig.10. Plots of lnk_2 *versus* 1/T for Cr(VI) on Fe_3O_4, Fe_3O_4/P and Fe_3O_4/G.

Table 3. The constants of adsorption isotherms

Sample	Langmuir			Freundlich			Temkin		
	q_{max}/ (mg·g^{-1})	K_L/ (L·mg^{-1})	R^2	K_F/ mg·g^{-1}(L·mg^{-1})$^{1/n}$	n	R^2	K_T/ (L·g^{-1})	B	R^2
Fe_3O_4	39.5	0.00940	0.995	4.67	1.89	0.993	0.0835	25.47	0.983
Fe_3O_4/P	62.5	0.00357	0.992	8.99	2.45	0.985	0.388	15.62	0.974
Fe_3O_4/G	78.5	0.000615	0.998	15.17	2.70	0.986	0.653	19.03	0.987

Table 4. Kinetic constants of activation energy in adsorption

C_0/ (mg.L^{-1})	T/(K)	Fe_3O_4			Fe_3O_4/P			Fe_3O_4/G		
		q_e / (mg·g^{-1})	k_2 / (min^{-1})	R^2	q_e / (mg·g^{-1})	k_2 / (min^{-1})	R^2	q_e / (mg·g^{-1})	k_2 / (min^{-1})	R^2
50	298.15	15.66	0.0192	0.995	19.29	0.0211	0.987	20.37	0.0236	0.996
50	303.15	10.05	0.0305	0.993	14.93	0.0493	0.995	18.29	0.0384	0.989
50	308.15	8.37	0.0374	0.988	11.85	0.0578	0.992	15.71	0.0478	0.992

Regeneration of the adsorbent

Since the adsorption of Cr(VI) onto adsorbent was a reversible process, the regeneration of the adsorbed nanocomposites was conducted using the dipping of NaOH (0.1 mol/L) aqueous solution and magnet separation. The nanocomposite was repeatedly putted into 50mg/L solution of Cr(VI) for adsorption and taken out for regeneration. In each cycle, the percentage of removal (R_r) was calculated using Eq.(1) for the adsorption process. The regeneration results were shown in Fig.11. The adsorption efficiency could still remain high after five cycles, which indicated that Fe_3O_4/carbonaceous had a good capacity of regeneration and repeatability.

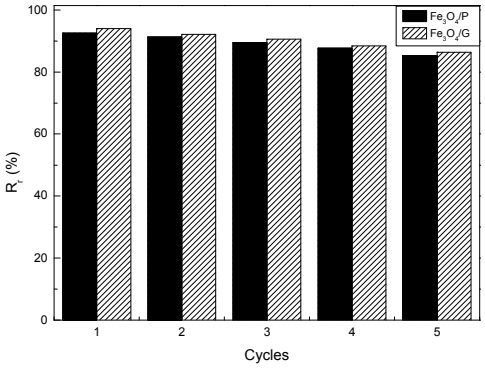

Fig. 11. Adsorption–desorption cycles of Fe_3O_4/P and Fe_3O_4/G for Cr(VI).

Conclusions

Fe_3O_4 nanoparticles hybridized with carbonaceous materials, such as pinecone and graphene, were successfully synthesized by a facile hydrothermal method, which could be applied for Cr (VI) removal in aqueous solution. The nanocomposites were characterized by XRD, SEM and N_2 adsorption-desorption isotherm. Due to the combination of pinecone and graphene, both the surface properties and morphologies of Fe_3O_4 were modified. Fe_3O_4 spherical particles were distributed and firmly anchored on loose surface of pinecone or wrinkled graphene layers. The specific surface area increased from 23.85 to 27.86 and 121.17 $m^2 \cdot g^{-1}$ for Fe_3O_4/P and Fe_3O_4/G respectively. It enhanced the adsorption capacity for Cr (VI) of Fe_3O_4/P (62.5mg·g^{-1}) and Fe_3O_4/G (78.5mg·g^{-1}). The kinetics and isotherm study showed that the pseudo-second-order kinetic and Langmuir isotherm models could well fit the adsorption data. There were three steps in the adsorption process, such as the instantaneous adsorption step, the intraparticle diffusion and the final equilibrium stage. The reaction rate decreased along with temperature increasing, which indicated the adsorption for Cr (VI) was an exothermic process. The E_a were 34.39, 25.77 and 34.92 kJ·mol^{-1} for Fe_3O_4, Fe_3O_4/P and Fe_3O_4/G respectively, which illustrated the adsorption of Cr(VI) onto the surface of nanocomposite was a physical process. In no more than 5h, about 92.6% and 94% Cr(VI) were desorbed from Fe_3O_4/P and Fe_3O_4/G, respectively, which indicated the adsorption-desorption process for Cr(VI) was reversible, The results demonstrated that Fe_3O_4/P and Fe_3O_4/G exhibited excellent adsorption performance in the removal of Cr(VI). It was proved that carbonaceous materials, such as pinecone or graphene, could enhance the adsorption efficiency of Fe_3O_4, which might be used as adsorbent to remove heavy metal in industry effluent.

Acknowledgements

This work has been supported by The National Natural Science Foundation of China (41340037) and the scientific research program of Shandong Province (2013G0021701, 2014GGH217001).

Notes and references

1 N. K. Srivastava, C. B. Majumder, *J. Hazard. Mater.*, 2008, **151**, 8.
2 C. Y. Chang, X. H. Xu and C. P. Liu, *Environ. Prog.*, 2014,**16**, 1790.
3 N. N. Thinh, P. T. B. Hanh, L. T. T. Ha, Le N. Anh, T. V. Hoang, V. D. Hoang, L. H. Dang, N. V. Khoi, T. D. Lam, Mat. Sci. Eng. C, 2013, **33**, 1214
4 L. F. Feng, W. Qi, *J. Environ. Manage.*, 2011, **92**, 407.
5 L. Zhou, C. Gao W. J. Xu, *ASC Appl. Mater. Interfaces*, 2010, **2**, 1483.
6 A. Maleki, B. Hayati, M. Naghizadeh, S. W. Joo, J. Ind. Eng. Chem., 2015, **28**, 211
7 A. Adamczuk, D. Kolodynska, Chem. Eng. J., 2015, **274**, 200.
8 Z. Lv, C. Liang, J. Cui, Y. Zhang and S. Xu, RSC Adv., 2015, **5**, 18213
9 V. Kumari, M. Sasidharan and A. Bhaumik, Dalton Trans., 2015, 44,1924
10 G. X. hui, Z. jie, *Environ. Technol.*, 2005, **7**, 409.
11 C. Yang, G. Wang and Z. Y. Lu, *J. Mater. Chem.*, 2005,**15**, 4252.
12 G. Chen, C. Qiao, Y. Wang, and J. Yao, Ind. Eng. Chem. Res. 2014, **53**, 15576
13 A. Masoumi, M. Ghaemy and A. N. Bakht, *Ind. Eng. Chem. Res.,* 2014, **53**, 8188.
14 W. Jiang, Q. Cai, W. Xu, M. Yang, Y. Cai, D. D. Dionysiou, and K. E. O'Shea, Environ. Sci. Technol. 2014, **48**, 8078
15 D. H. K. Reddy, S. Lee, Adv. Colloid Interfac. 2013, **68**, 201.
16 D. H. K. Reddy, S. Lee, Colloid Surface A, 2014, **454**, 96.
17 G. Yang, L. Tang, G. Zeng, Y. Cai, J. Tang, Y. Pang, Y. Zhou, Y. Liu, J. Wang, S. Zhang and W. Xiong, Chem. Eng. J., 2015, 259,854
18 L. Tang, S. Zhang, G. Zeng, Y. Zhang, G. Yang, J. Chen, J. Wang, J. Wang, Y. Zhou and Y. Deng, J. Colloid Interface Sci. 2015, **445**: 1
19 Z. Jiang, Y. Liu, G. Zeng, W. Xu, B. Zheng, X. Tan and S. Wang, RSC Adv., 2015, **5**, 25389
20 C. Wu, J. Fan, J. Jiang and J. Wang, RSC Adv., 2015, **5**, 47165
21 F. Perreault, A. F. Faria and M. C. Elimelech, *Chem. Soc. Rev.*, 2015, **9**, 1039.
22 M. C. Liu, T. Wen, X. L. Wu, C. L. Chen, J. Hu, J. Lia and X. K. Wang, Dalton Trans., 2013, **42**, 14710.
23 H. T. Yu, Y. C. Li, X. H. Li, L. Z. Fan and S. H. Yang, *J. Mater. Chem.,* A, 2014, **2**, 15763.
24 X. F. Han, L. Zhang and C. Z. Li, *RSC Adv.*, 2014, **4**, 30536.
25 Z. Z. Guang, Y. H. Jiang and L. Fei, Chin. *J. Inorg. Chem.*, 2011, **9**, 1753.
26 Z.G. Ke, Q. Huang, H. Zhang, Z.L. Yu, Environ. Sci. Technol., 2011, **45**, 7841.
27 D. Ying,L. Jing,S. Lei , *J. Mater. Chem. A*, 2015, **10**, 1039.
28 V. Stengl, J. Bludska and F. Oplustil, Mater. *Res. Bull.*, 2011, **46**, 2050.
29 I. A. W. Tan, A. L. Ahmad and B. H. Hameed, *J. Hazard. Mater.*, 2009, **164**, 473.
30 S. Rengaraj, Y. Kim and C. K. Joo, *J. Colloid Interface Sci.*, 2004, **273**, 14.
31 A. Gajic, H. G. Ramke and A. Hendrickset, *Biomass Bioenergy*, 2012，**47**：250.
32 E. L. Grabowska, G. Gryglewicz, *J. Colloid Interface Sci.*, 2005, **284**: 416.
33 Y. Onal, C. Akmil-Bar and D. Eren, *J. Hazard. Mater.*, 2006, **128**: 150.
34 T. Rui , Y. Gang and L. Hang, *Phys. Chem. Chem. Phys.*, 2014,**16**, 8828.

The Efficient Adsorption Removal of Cr (VI) by Using Fe_3O_4 Nanoparticles Hybridized with Carbonaceous Materials

Carbonaceous materials, such as pinecone and graphene, have been hybridized with Fe_3O_4 to modify its surface properties and enhance its adsorption efficiency for Cr(VI) removal in aqueous solution. Due to the combination of pinecone and graphene, both the surface properties and morphologies of Fe_3O_4 were modified. It enhanced the adsorption capacity for Cr (VI) of Fe_3O_4/P ($62.5 mg \cdot g^{-1}$) and Fe_3O_4/G ($78.5 mg \cdot g^{-1}$). The adsorption of Cr(VI) onto the surface of nanocomposites was proved to be a physical endothermic process, which can be fit by pseudo-second-order kinetic and described by the Langmuir isotherm models.